

Use of ATLAS Visual and Thermal Imagery to Study the Urban Heat Island Effect in San Juan, Puerto Rico

Ana J. Picón-Feliciano
Departamento de Ingeniería Eléctrica y Computadores
Universidad de Puerto Rico, Recinto de Mayagüez
P.O Box 5328, Mayagüez PR 00681
ana.picon@ece.uprm.edu

Abstract—This research is focused in the study of local climate effects due to urbanization in tropical coastal cities. With the use of remote sensing technology, climate changes due to urban growth can be detected. The clearest local indicator of climate changes due to urban growth is a urban/rural convective circulation known as Urban Heat Islands (UHI). The main scientific objective of this research is to investigate the impact of the fast urbanization in the local climate of tropical coastal cities that is related to UHI. The Airborne Thermal and Land Applications Sensor (ATLAS) from NASA/Stennis that operates in the visual and IR bands was used as the main sensor for this study with the objective of investigating the Urban Heat Island (UHI) in San Juan, Puerto Rico. Temperatures as high as 60°C over the developed areas differ from temperatures over vegetated areas of more than 30°C during daytime. The UHI curve over the San Juan area is a clear evidence of the characteristic high temperature domes over urbanized areas. Correlations between temperature and albedo provide additional information of the different surface energy budget components. The Normalized Difference Vegetation Index (NDVI) was also estimated to separate the land use and land cover components over the San Juan area. Results from this research have shown outstanding evidence of elevated surface temperatures over the urban landscape and clearly validate the development of UHI in San Juan, Puerto Rico.

Keywords—surface, temperature, albedo, energy, urbanization, NDVI, land use.

I. INTRODUCTION

It is difficult to imagine that cities in small tropical islands show local climate change effects similar to those in great continental cities. It was recently discovered in (González et al., 2006) that this might be the case for the city of San Juan, Puerto Rico, a relatively affluent coastal tropical city of nearly 2 million inhabitants. The main scientific objective of this research is to investigate the relationship between urban growth, land cover change, and the development of the urban heat island phenomenon over a tropical coastal city; San Juan, Puerto Rico. Also study the overall effects of urban development on surface energy budget characteristics across the urban landscape through time at nested spatial scales from local to regional. A field campaign was designed and executed in February 2004 to validate this phenomenon. The field campaign included on-board high resolution infrared sensors, ground stations, and upper air balloons. The Airborne Thermal and Land Applications Sensor (ATLAS) from NASA/Stennis that operates in the visual and IR bands was used as the main sensor for this field campaign with the objective of investigating the Urban Heat Island (UHI) in San Juan, Puerto Rico. Infrared sensor measurements can provide land

surface parameters such as temperature and albedo. These two parameters are the key elements in the study of urban heat island. A brief review of relevant works is provided in this section.

Landsat 7 has been used in urban heat island studies in the city of Atlanta (Poreh, 1996). This sensor has a spatial resolution of 60 m in the spectral range of 10.40 to 12.5 μm . One constraint of the instrument is the temporal variation due to overpasses through Puerto Rico which is every 16 days. To retrieve surface temperature, band 6 is adjusted with an atmospheric model or profile. (Fukui et al., 2002) presented a study based on the surface temperature distribution and the urban structure in Tokyo using the Advanced Spaceborne Thermal Emission and Reflection Radiometer (ASTER) and LIDAR data. ASTER has a spatial resolution of 90m in the spectral range of 8.125 to 8.825 μm , 8.925 to 9.275 μm and 10.25 to 11.65 μm . In this study, two different scenes from ASTER were used to calculate the surface temperature via the temperature/emissivity separation (TES) algorithm. The correlation of the surface temperature and the urban structure shows the impact of green areas on the urban heat environment and the falling of surface temperature in tall buildings during daytime and increasing of surface temperature during nighttime. Furthermore, NOAA Advanced Very High

Resolution Radiometer (AVHRR) thermal IR images have been studied to understand the urban microclimates of cities such as Paris and Los Angeles (Dousset and Gourmelon, 2001). This radiometer has a spatial resolution of 1km and two thermal bands in the spectral range of 10.3 to 11.3 μ m and 11.5 to 12.5 μ m. To retrieve surface temperature, it uses a split window equation. MODIS has the same resolution as NOAA AVHRR but has the capability of acquiring data over 36 spectral bands. (McCabe et al., 2001) compared MODIS and NOAA AVHRR land surface temperatures with ground based infrared thermometry measurements made in Tomago, Sandbeds, north of Newcastle, Australia. Comparisons show good agreement between MODIS, NOAA AVHRR and the infrared thermometer. (Quattrochi and Luvall) explain in detail the surface temperature retrieval from these instruments. No major research has been reported where remote sensing images are used to investigate the urban climate in tropical and subtropical regions.

The remaining parts of the paper are organized as follow: Section II presents the theoretical aspects and the post-processing of the ATLAS data, Section III presents results obtained from the San Juan area, Section IV includes the conclusions and the future work, and finally, Section V includes the references.

II. ENERGY SURFACE BUDGET DEFINITIONS AND ATLAS DATA POST-PROCESSING

The Airborne Thermal and Land Applications Sensor (ATLAS) of NASA/Stennis operates in the visible and infrared bands. The ATLAS can detect 15 multispectral channels of the radiation through the visible, near infrared, and thermal spectrums (see Figure 1 and 2). The sensor also incorporates the active sources of calibration needed for all bands. The data is corrected for the atmospheric radiation, and georectified before the analysis of the data is performed. The ATLAS sensor has been used in other field campaigns to investigate the UHI in Atlanta, Salt Lake City, Baton Rouge, and Sacramento, all in the continental mass of the United States of North America described in (Luvall et al., 2005).

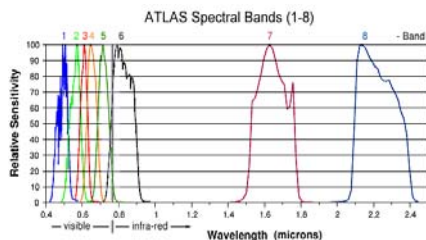


Figure 1. Spectral resolution of the airborne thermal and land applications sensor(ATLAS). Bands 1-8.

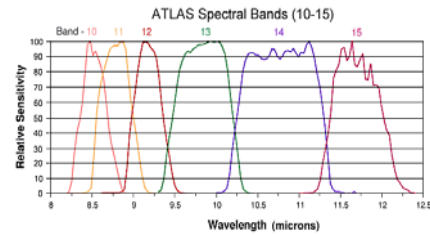


Figure 2. Spectral resolution of the airborne thermal and land applications sensor(ATLAS). Bands 10-15.

The ATLAS Mission of San Juan, Puerto Rico was conducted during February of 2004 to investigate the impact of the urban growth and landscape in the climate of this tropical city. The flight plan of the mission covered the metropolitan area within San Juan, the national forest of El Yunque to the east of San Juan, the city of Mayagüez in the west coasts of Puerto Rico, and the Arecibo Observatory located in the north-central coast, for a total of 25 flight lines. The downtown area of San Juan, Hato Rey, was covered in a horizontal resolution of 5 meters in flights during the day and during the night. The remaining areas of the city were covered in 10 meters of resolution. The flights were executed between the 11 and the 16 of February of 2004. In order to analyze the existence of an urban heat island in San Juan, and to support the data of the ATLAS sensor, several experimental campaigns for data collection were designed and conducted by different teams, in addition diverse numerical experiments were performed that helped to understand the phenomenon and its characteristics.

The atmospheric corrections needed to produce calibrated data sets from ATLAS involve a complex procedure. They require direct measurements of the atmosphere extinction coefficients by wavelength and profiles of atmospheric temperatures and water vapor. ATLAS instrument characteristics and calibration are also required. Figure 3 details the process flow followed for this project including resulted images from every relevant routine. A combination of software was used for the processing, including the public domain image processing/remote sensing package ELAS (Beverley and Penton, 1989) and a series of custom programs, Watts and Energy from ELASII (Rickman et al., 2000).

MODTRAN4 (Berk et al., 1999) was used to model the atmospheric radiance and transmittance using input from radiosonde data and shadow band radiometers. (Rickman et al., 2000) details the procedure for calibrating the ATLAS sensor to produce the system transfer function to convert digital values (DV) into radiance measurements. These procedures produce ATLAS data files that are in physical units of energy. These files are used for

the generation of files which derive albedo and surface temperature.

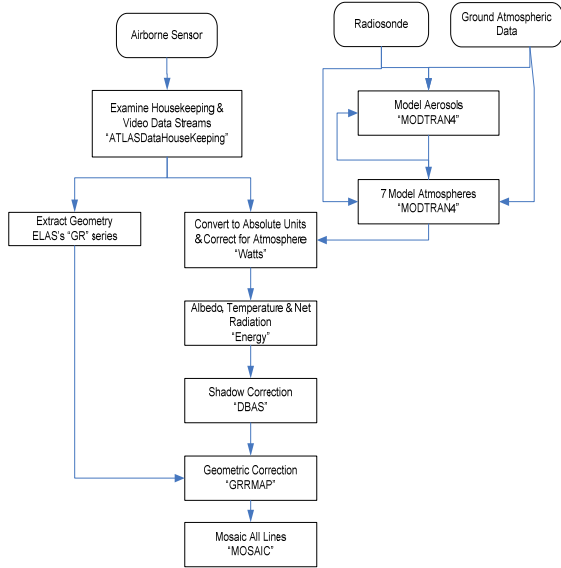


Figure 3. ATLAS overall data-processing flowchart.

Surface temperature is a major component of the surface energy budget. In (Oke, 1987) the use of energy terms in modeling surface energy budgets allows the direct comparison of various land surfaces encountered in a landscape, from vegetated (forest and herbaceous) to non-vegetated (bare soil, roads, and buildings). The partitioning of energy budget terms depends on the surface type. In natural landscapes, the partitioning is dependent on canopy biomass, leaf area index, aerodynamic roughness, and moisture status, all of which are influenced by the development stage of the ecosystem. In urban landscapes, coverage by man-made materials substantially alters the surface energy budget. The net all-wave radiation balance (W/m^2) of landscape canopies can be determined as follows (Oke, 1987).

The net solar radiation, K^* , is given by

$$K^* = (1-a)(K\downarrow) \quad (1)$$

where a is the site albedo and $K\downarrow$ is the incoming solar radiation. The albedo is defined as

$$a = (K\uparrow)/(K\downarrow) \quad (2)$$

where $K\uparrow$ is the reflected solar radiation. The long wave energy emitted from a surface ($L\uparrow$) is dependent on surface temperature:

$$L\uparrow = \varepsilon[\sigma T^4] \quad (3)$$

where ε is the emissivity and σ is the Stefan-Boltzman constant ($5.7 \times 10^{-8} W/m^2 \cdot K^4$) and T is the land surface temperature (Kelvin). The net long wave radiation at the surface, L^* , is given by

$$L^* = L\downarrow - L\uparrow \quad (4)$$

where $L\downarrow$ is the long wave radiation from the atmosphere. The net all-wave radiation, Q^* , can be given as:

$$Q^* = K^* + L^* \quad (5)$$

Net radiation, under most conditions, represents the total amount of energy available to the land surface for partitioning into non-radiative processes (mass heating, biological synthesis, etc.) at the surface. It is the amount of energy the system holds on to and degrades. In vegetated areas the amount of net radiation is dependent upon vegetation type and varies with canopy leaf area and structure. The net radiation may be expressed as the sum of these non-radiative fluxes:

$$Q^* = \lambda E + H + G \quad (6)$$

where H is the sensible heat flux, λ is the latent heat of vaporization of water, E is the transpiration flux and G is the energy flux into or out of storage (both canopy and soil). The partitioning λE , H and G are also dependent on the makeup of the surface. Both the physiological control of moisture loss (stomatal resistance) and leaf/canopy morphology for vegetation determines how Q^* is partitioned among λE , H , and G . For urban surfaces the coverage of both man-made materials and vegetation results in a heterogeneous mixture of surfaces which determine the partitioning of energy. The ATLAS remotely sensed data allows the measurement of important terms in the radiative surface energy budget: $K\uparrow$ and $L\uparrow$ on a urban landscape scale. When combined with output from MODTRAN4 (Berk et al., 1999) atmospheric radiance models the remaining terms and Q^* can be determined.

III. MATERIALS AND METHODS

The image processing software that was used in this laboratory was ENVITM. Images from San Juan, Puerto Rico at a spatial resolution of 10 meters, Hato Rey at a spatial resolution of 5 meters and El Yunque at a spatial resolution of 10 meters were acquired by ATLAS. The dataset products were WATTS MOSAIC and ENERGY MOSAIC. Since the ATLAS datasets are not compatible with the ENVITM software, new ENVI formatted headers were created (see Appendix 1 for more information). Different tasks were performed to obtain information about the urban climate phenomena studied.

1) Normalized Difference Vegetation Index

The first step was to open and interpret the WATTS MOSAIC image to examine the Red and Infrared bands. The second step was to select the Red channel that absorbs more and the Infrared channel that reflects more. The third step was to calculate the

NDVI for the image using by entering the equation (7) in the Band Math basic tool of ENVI™.

$$\text{NDVI} = ((\text{float}(\text{b6})) - (\text{float}(\text{b4}))) / ((\text{float}(\text{b6})) + (\text{float}(\text{b4}))) \quad (7)$$

where b4 is the spectral reflectance in the Red Visible Band and b6 is the spectral reflectance in the Near-Infrared Band from the WATTS MOSAIC datasets. A mask was prepared to filter values out of the range between 0 and 1 by using the Build Mask basic tool. A scale bar was added to the image by using the ENVI™ Color Tables under the Color Mapping tool and then a Color Ramp Object under the Annotation tool from the Overlay menu.

2) *Multispectral Classification*

The first task was to perform unsupervised classification of the WATTS MOSAIC datasets. ENVI™ provides two different unsupervised classifiers: isodata and k-means.

As explained by the ENVI™ helper, isodata calculates class means evenly distributed in the data space and then iteratively clusters the remaining pixels using minimum distance methods. Each iteration recalculates means and reclassifies pixels with respect to the new means. Iterative class splitting, merging, and deleting are done based on the input threshold parameters. All pixels are classified to the nearest class unless a standard deviation or distance threshold is specified, in which case some pixels may be unclassified if they do not meet the selected criteria. This process continues until the number of pixels in each class changes by less than the selected pixel change threshold or the maximum number of iterations is reached. The isodata classification of the images was realized with the default parameters.

In theory, k-means is an algorithm to cluster objects based on attributes into k partitions. The idea of the algorithm is to find the centers of natural clusters in the data. The objective is to minimize total intra-cluster variance, or, the squared error function.

$$V = \sum_{i=1}^k \sum_{x_j \in S_i} |x_j - \mu_i|^2 \quad (8)$$

where there are k cluster S_i , $i=1,2,\dots,k$ and μ_i is the centroid or mean point of all the points $x_j \in S_i$. The procedure is similar to isodata. In the case of k-means, the images were classified for 10 classes and 2 iterations were done.

The second task was to perform supervised classification of the subset image by using the minimum distance, Mahalanobis distance and maximum likelihood classifiers. As explained by the ENVI™ helper, the minimum distance technique

uses the mean vectors of each endmember and calculates the Euclidean distance from each unknown pixel to the mean vector for each class. All pixels are classified to the nearest class unless a standard deviation or distance threshold is specified, in which case some pixels may be unclassified if they do not meet the selected criteria. The Euclidean distance or Euclidean metric (defined in Fukunaga, 1990) is the distance between two points $P = (p_1, p_2, p_3, \dots, p_n)$ and $Q = (q_1, q_2, q_3, \dots, q_n)$, in Euclidean n-space, is defined as:

$$D_E(p, q) = \sqrt{\sum_{i=1}^n (p_i - q_i)^2} \quad (9)$$

Maximum Likelihood (ML) is a parametric classifier that uses the training samples to estimate some parameters such as mean vector and covariance matrix. This is the most common supervised method used with remote sensing image data (Richards, 1993). This method involves specifying the joint probability distribution function for the sample data. Under relatively weak assumptions, usually called regularity conditions, maximum likelihood estimates are consistent, asymptotically normal, and efficient. Consistency means that as the sample size increases, the ML estimate tends in probability to the true parameter value. Moreover, for large sample size, the ML estimate will have an approximate normal distribution centered on the true parameter value. The spectral classes for an image be represented by $\omega_i = 1, \dots, M$ where M is the total number of classes. The probability $p(\omega_i | x)$ gives the likelihood that the correct class is ω_i for a pixel at position X. Then, the classification is performed according to $X \in \omega_i$ if $p\left(\frac{\omega_i}{x}\right) > p\left(\frac{\omega_j}{x}\right)$ for all $j \neq i$. The

Multivariate Normal Class Model, if we assumed N bands is:

$$p\left(\frac{x}{\omega_i}\right) = (2\pi)^{-\frac{N}{2}} |\Sigma_i|^{-\frac{1}{2}} \exp\left\{-\frac{1}{2}(x - m_i)' \Sigma_i^{-1} (x - m_i)\right\} \quad (10)$$

where m_i and Σ_i are the mean vector and covariance matrix of the data in class ω_i .

Mahalanobis distance is a parametric classifier that uses the training samples to estimate some parameters such as mean vector and covariance matrix. It is a distance measure introduced by P. C. Mahalanobis in 1936. It is based on correlations between variables by which different patterns can be identified and analyzed. It differs from the Euclidean distance in that it takes into account the correlations of the data set and is scale-invariant, that means that it's not dependent on the scale of measurements. The

Mahalanobis distance from a group of values with mean $\mu = (\mu_1, \mu_2, \mu_3, \dots, \mu_n)^T$ and covariance matrix Σ for a multivariate vector $x = (x_1, x_2, x_3, \dots, x_n)^T$ is defined as:

$$D_M(x) = \sqrt{(x - \mu)^T \Sigma^{-1} (x - \mu)} \quad (11)$$

A ROI (region of interest) file was prepared with 5 classes: ocean, lakes, forest, agriculture and cities. This ROI file will be used as training samples for the supervised classifiers. By result, three different images were produced. Every image created was saved in ENVITM and jpeg format. The final task is to compare the images and discuss about the similarities and differences between the results.

3) Correlations between surface parameters

Albedo alone does not truly reflect how the lands' surface partitions energy. A good example is the comparison between vegetated and asphalt surfaces (see Table 1). Both surfaces have a low albedo, but the asphalt surface temperature can be over 34°C greater than the vegetated surface. If the surface temperature is included the needed additional information to assess the "urban fabric" of the city is provided. The surface temperature and albedo classifications represent a functional classification of that surface, that can readily be incorporated into the surface parameterization of meteorological and air quality models. Within each city, each land use has a unique "energy print" that is directly physically related to how that surface is processing energy. These "energy prints" of the land use are unique for each city.

Surface	Albedo %
Water	5-10
Desert	25-30
Fresh snow	80-90
Old snow	45-70
Green forest	5-10
Green leaves	5-25
Clouds (average)	50-55
Clouds < 150 m thick	25-63
Clouds 150-300 m thick	45-75
Clouds 300-600 m thick	59-84
Sea ice	30-40
Bitumen road	5-10

Table 1. Albedo values for different surfaces.

Surface parameters such as the temperature and albedo were obtained from the ENERGY MOSAIC datasets. The first steps to visualize this correlation is by selecting the two surface parameters and displaying them in ENVITM, then go to Image Menu/Tools/2-D Scatter plots and select the X-band and the Y-band to be displayed. A window with a scatter plot will appear. By moving the window box through the image, one can select the area to be observed.

4) Urban Heat Island Curve

To show evidence of the elevated temperature domes that are characteristic of urban areas with surrounding rural areas that present low temperature patterns, a UHI curve must be plotted. First, the surface temperature must be selected from the ENERGY MOSAIC datasets and displayed in ENVITM. Then go the Image Menu/Tools/Profile/Arbitrary Profile (Transect) and select the path over the image to be observed.

IV. RESULTS and DISCUSSION

NDVI results from San Juan, Puerto Rico show the dominant city (white pixels) surrounded by rural areas (mostly green pixels). Oceans, lakes and rivers can be well distinguished with black pixels. Figure 4 show the NDVI generated image by ENVITM for the San Juan Metropolitan area. In Figure 5, a different contrast between forest and coastal cities is observed. El Yunque, at the East of Puerto Rico, predominates with green pixels surrounded by coastal cities in white pixels. Results from Hato Rey also show similar relation between pixels (see Appendix 2).

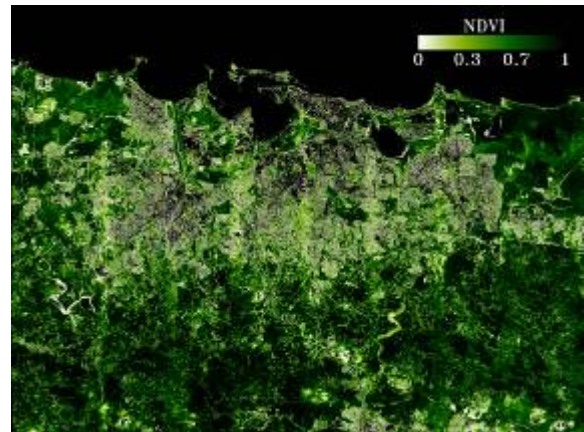


Figure 4 NDVI values for the San Juan Metropolitan area and its surroundings.

Two different tasks were performed: one for unsupervised classification and the second for supervised classification. Figure 6 shows the

classified image using the isodata classifier and figure 7 shows the classified image using the k-means classifier. What is more obvious is that ocean is very well classified in the three images. The isodata classifier detects better the vegetation and the cities pixels.

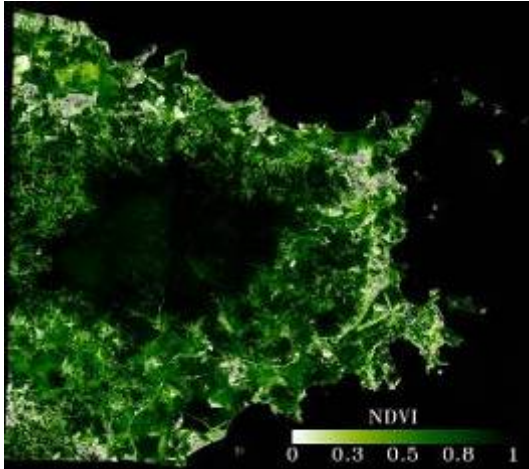


Figure 5 NDVI values for the East of Puerto Rico.

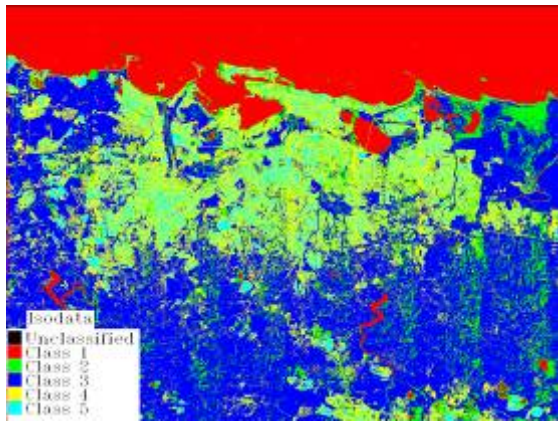


Figure 6 Unsupervised classification using the Isodata classifier.

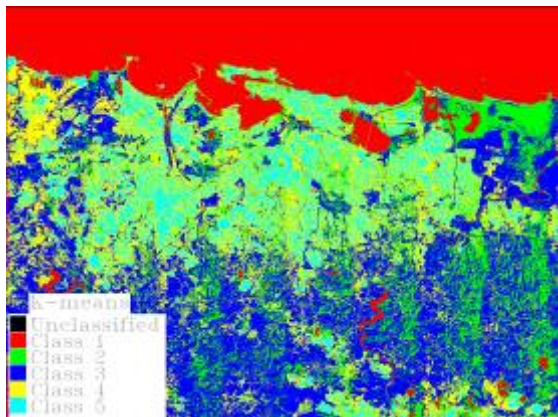


Figure 7 Unsupervised classification using the K-means classifier.

The supervised classification of the images shows a different scenario in which 5 classes are selected: ocean, lakes, forest, agriculture and cities. Based on these samples, the supervised algorithm is executed. Figure 8-10 shows the classified image based on minimum distance, Mahalanobis distance and maximum likelihood, respectively. Minimum distance didn't make distinction between ocean and lakes pixels. On the other part, maximum likelihood shows a better overall performance. Also agriculture and forest pixels are discriminated better in the maximum likelihood classified image.

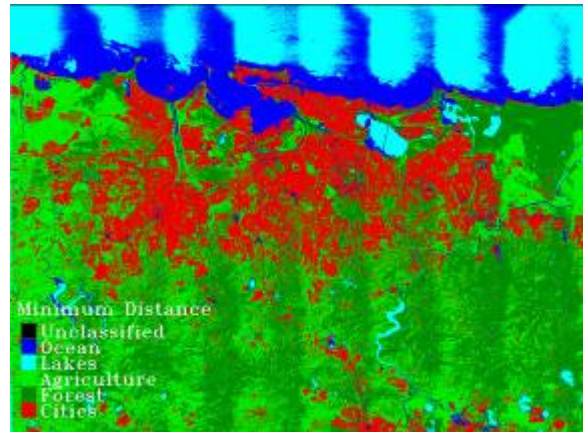


Figure 8 Supervised classification using the Minimum distance classifier.

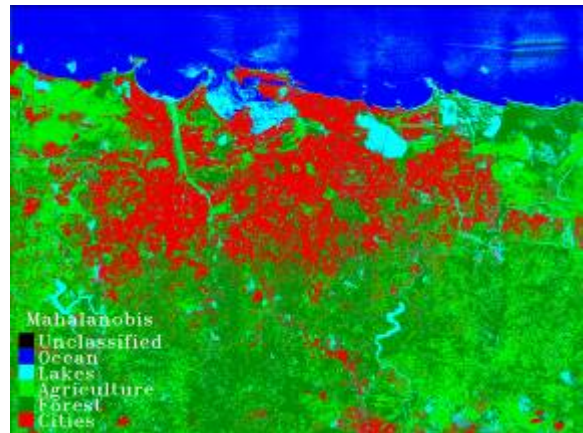


Figure 9 Supervised classification using the Mahalanobis distance classifier.

Compared to the unsupervised classifiers, this one works better for the distinction of cities and vegetation. By just looking at the classified images, it seems that the supervised minimum distance classify better. In this type of exercise, the unsupervised classifiers were not effective. Another important observation is the selection of samples to be trained by the classifier, they make a big difference. One important observation about the

images is that river pixels did not vary from highway pixels which seem to be a problem to discriminate one class from the other. One good recommendation is to use surface temperature ranges for rivers and roads when selecting the ROIs. (Fukunaga, 1990) proves that second-order classifiers (such as minimum distance and maximum likelihood) can discriminate very well by using a quadratic relation between training samples and dimensionality. On the other side, unsupervised classifiers like isodata and k-means do not depend on the samples and it may result in a disadvantage. In this case, dimensionality is not tested but it seems that a combination of dimensionality and training samples can lead to a better classification. This might be a good future exercise.

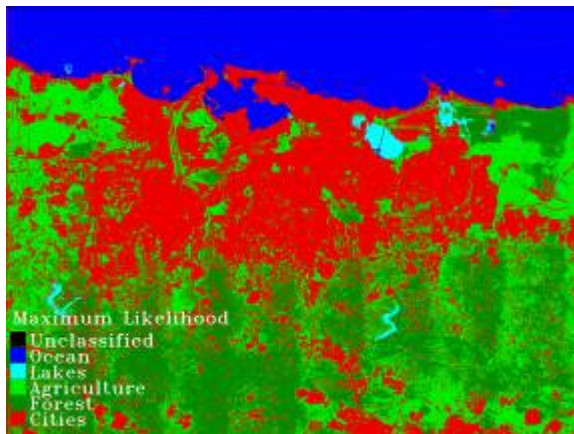


Figure 10 Supervised classification using the Maximum Likelihood classifier.

The San Juan Metropolitan zone includes vegetated areas such as the Experimental Station, lake, airport, coastal industrial areas such as Cataño and central building areas. Differences in temperatures indicate a heat pattern dominating urban and coastal areas. Vegetated areas reflect albedo values around 0.07 and 0.15. Water bodies reflect albedo values around 0.06 and 0.3. Albedo values higher than 0.78 correspond to cloud bodies. Since the San Juan Metropolitan zone includes vegetation, water bodies, residential, industrial and central building components, the surface energy budget can be evaluated by observing the energy contribution of each component to the whole UHI energy print. The way each surface partitions energy is unique depending on material type, vegetated or non-vegetated, water status, atmospheric vapor deficits, and the relative mixtures and arrangements of the various components of that surface. Figure 11 shows an image of San Juan with its relative surface energy components. Individual vegetated components such as the Experimental Station Area which is one of the

most vegetated areas in the city shows a very low contribution of surface temperature vs albedo. Generally the industrial areas had the highest albedo, and the hottest temperatures. The park areas show the lower albedo (not always the lowest) and lowest temperatures. Residential areas reflect low albedo values in a range from low to high surface temperatures. The airport area is mostly an asphalt surface that can be very hot in terms of temperature. The hottest surfaces correlate with roofs and asphalt pavements. See Appendix 2 for more results.

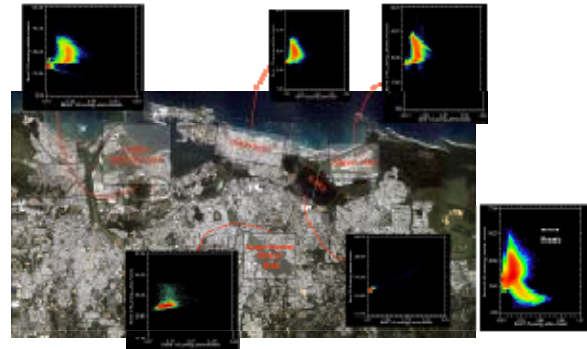


Figure 11 San Juan scatter plots that identifies the energy portions from urbanized and vegetated areas at different spots.

Finally, the evidence of UHI over the San Juan area can be represented by the temperature curve (see Figure 12). The concept of UHI domes over the city can be represented by using the Transect tool of ENVI™. Using this method with remote sensing data can be more convenient than selecting points and creating an Excel graph.

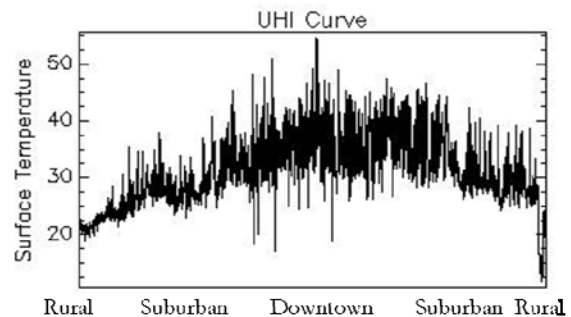


Figure 12 Temperature curve for the San Juan Metropolitan area showing domes of elevated temperatures over the downtown area.

V. CONCLUSIONS

The work presented is part of a comprehensive investigation of the impact of land use for urbanization on the environment of a city located on a small tropical island, in this case, San Juan, Puerto

Rico. The ATLAS field campaign conducted in February 2004 validates the development of UHI showing temperatures as high as 60°C with temperature differences between the developed and vegetated areas of more than 30°C during daytime. Classification methods are very important in the analysis of UHI data. Supervised classifiers show a higher level of performance when detecting surface components from a city. Correlation between surface temperature and albedo show the thermal characteristic of energy prints. These prints represent the surface energy portion from the urban city component that contributes to the total surface energy budget. Surface temperature, albedo and NDVI results from San Juan show evidence of the urban growth impact in a tropical coastal city. Because ATLAS also has superior spectral resolution within the thermal IR channels, it offers the potential to make accurate measurements of thermal responses for different landscape characteristics and their corresponding land-atmosphere interactions over small wavelength regions. Energy prints from the different components in a urban city represent the surface energy portion that contributes to the total surface energy budget. Future work will include the validation of the supervised classifiers to create a table with the characteristic surface temperature and albedo for every surface.

VI. ACKNOWLEDGEMENTS

Special thanks to the ATLAS mission campaign developer: the NASA Global Hydrology and Climate Center (NGHCC), Huntsville, AL and NASA Stennis Space Center and the Principal Investigator, Dr. Jeffrey C. Luvall.

VII. REFERENCES

- Berk, A, G.P. Anderson, P.K. Acharya, J.H. Chetwynd, L.S. Bernstein, E.P. Shettle, M.W. Matthew, and S.M. Adler-Golden, 1999. MODTRAN4 Users Manual. *Air Force Research Laboratory, Space Vehicles Directorate, Air Force Materiel Command, Anscm AFB, MA 01731-3010.*
- Beverley, A.M., and Penton, P.G.; 1989. ELAS, Earth Resources Laboratory Applications Software Vol II, User Reference; *Earth Resources Lab. Report No. 183; NSTL, Mississippi.*
- Colleagues of remote sensing in education: <http://www.geografforlaget.dk/course/ENGLISH/basic/vejrsat.htm>.
- Dousset, B., and F. Gourmelon, 2001. Remote sensing applications to the analysis of urban microclimates. *IEEE/ISPRS Joint Workshop Remote Sensing and Data Fusion over Urban Areas*, 168-172.
- Fukui, Y., Y. Hirose, and N. Mushiake, 2002. A study on the surface temperature distribution and the urban structure in Tokyo with ASTER and LIDAR data. *Proceedings of Geoscience and Remote Sensing Symposium (IGARSS '02)*, 4:24-28.
- Fukunaga, K., 1990. *Introduction to Statistical Pattern Recognition*. San Diego, California, Academic Press, Inc.
- González, J. E., J. C. Luvall, D. Rickman, D. E. Comarazamy, and A. J. Picón, 2006. Urban heat Island an a Coastal Tropical City: Case Study In The Metropolitan Area Of San Juan, Puerto Rico, Book chapter in *Urban Remote Sensing*, ed. Q. Weng and D. Quattrochi, CRC Press.
- Luvall, Jeffrey C., Rickman, D., Quattrochi, D. And Estes, M.; 2005. Aircraft Based Remotely Sensed Albedo and Surface Temperatures for Three US Cities; Color Roofing: Cutting through the Glare, Roof Consultants Institute Foundation, Atlanta, GA.; 8 pp.
- McCabe, M.F., Prata, A.J. and J.D. Kalma, 2001. The Effects of Scale on Predictions of Land Surface Temperature from a variety of Remote Sensing Platforms. *Proceedings of Geoscience and Remote Sensing Symposium (IGARSS '01)*, 3: 9-13.
- Oke, T.R., 1987. *Boundary Layer Climates*. Cambridge University Press. 450 pp.
- Poreh, M., 1996. Investigation of heat islands using small scale models, *Atmospheric Environment*, 30: 467-474.
- Quattrochi, D. and J. C. Luvall. Thermal Remote Sensing in Land Surface Processes, CRC Press, ISBN 0415302242.
- Richards, J.A., 1993. *Remote Sensing Digital Image Analysis, An Introduction*. 2nd ed. New York Springer-Verlag.
- Rickman, D.L.; J. C. Luvall, and S. Schiller. 2000. An algorithm to atmospherically correct visible and thermal airborne imagery. *Workshop on Multi/Hyperspectral Technology and Applications*, Redstone Arsenal, Alabama.
- Wikipedia in English, Euclidean Distance: http://en.wikipedia.org/wiki/Euclidean_distance.
- Wikipedia in English, Mahalanobis Distance: http://en.wikipedia.org/wiki/Mahalanobis_distance.

APPENDIX 1

How to read ATLAS data in ENVI™

Because ATLAS data is written in formats not recognized by ENVI, several steps must be done to read ATLAS data. Raw data is written in .flat and .img formats. Atmospherically corrected data product is a .wats output from the ELAS software. Geometrically corrected data product is a .geo output from the ELAS software. Surface data product is an .energy output from the ELAS software.

In the File Menu, select Open Image File to open ENVI image files (flat binary files) or other binary image files of known format.

1. Select File → Open Image File.
2. When the Enter Data Filenames dialog appears, select the file to open by clicking on its name and clicking OK or Open.
3. When ENVI first opens a file, it requires specific information regarding the file characteristics. If the file is an ENVI format file, the necessary information is contained in a separate text header file. The text header file has the same name as the image file, but the file extension is .hdr.

If ENVI cannot find the header file (.hdr file) or other valid header information upon opening a file, the Header Info dialog box appears (see Figure 13). You must enter the required information into the dialog before an imported image can be displayed in ENVI. The information needs to be entered only once and is automatically stored into an ENVI header file in the input directory when the OK button at the bottom of the Header Info window is selected.



Figure 13 Header Info dialog box.

Use the Header Info dialog to enter this information:

- The **Samples** field displays the number of samples in the file.

- The **Lines** field displays the number of lines in the file.
- The **Bands** field displays the number of bands stored in the file.
- The **Offset** field displays the offset in bytes from the start of the file to where the actual data begins. (The **Offset** is sometimes known as the embedded header.)
- The **xstart** and **ystart** fields define the image coordinates for the upper left- hand pixel in the image. The default values are (1,1) so that the upper left hand pixel has an image coordinate of (1,1).
- Use the **Data Type** pull-down menu to select the appropriate data type (byte, integer, unsigned integer, long integer, unsigned long integer, floating point, double precision, 64-bit integer and unsigned 64-bit integer, complex, or double complex).
- Use the **Byte Order** pull-down menu to select the byte order of the data. This parameter varies by platform:
 - For DEC machines and PCs, select Host (Intel), for the host least significant first byte order.
 - For all other platforms, select Network (IEEE), for the network most significant first byte order.
- Use the **Interleave** menu to select the data storage order from these choices(see Table 2):
 - BSQ — band sequential
 - BIL — band interleaved by line
 - BIP — band interleaved by pixel

Table 1 Band storage order description.

File Format	Minor Frame	Major Frame
BSQ	# of samples (line)	# of samples by # of lines (band)
BIL	# of samples (line)	# of samples by # of bands
BIP	# of bands (spectrum)	# of bands by # of samples

All additional information stored in the ENVI Header is optional. To access this optional information, click the Edit Attributes button in the Header Info dialog. This optional information includes setting the default Z-Plot range, default stretch for display, entering georeferencing information, associated wavelengths and associated FWHM (full-width-half-maximum) values, sensor type, band names, and bad bands.

Map information is associated with georeferenced files. In ENVI, the term georeferenced refers to images that have been geometrically corrected (i.e., rectified) such that they conform to a known projection. To establish the georeferenced data coordinate system, you must know the sample and line coordinates of one pixel (the reference pixel), the pixel size, the map projection, and map coordinates of this pixel.

4. After the file is opened, the bands are listed in the Available Bands List.
5. In the Available Bands List, click on the Display #X button menu (where X is the number corresponding to the number in a display window's title bar) and select the display from the list.
6. To start a new display, select New Display from the button menu.
7. Click Load Band or Load RGB to load the selected bands into the active display (see Figure 14).

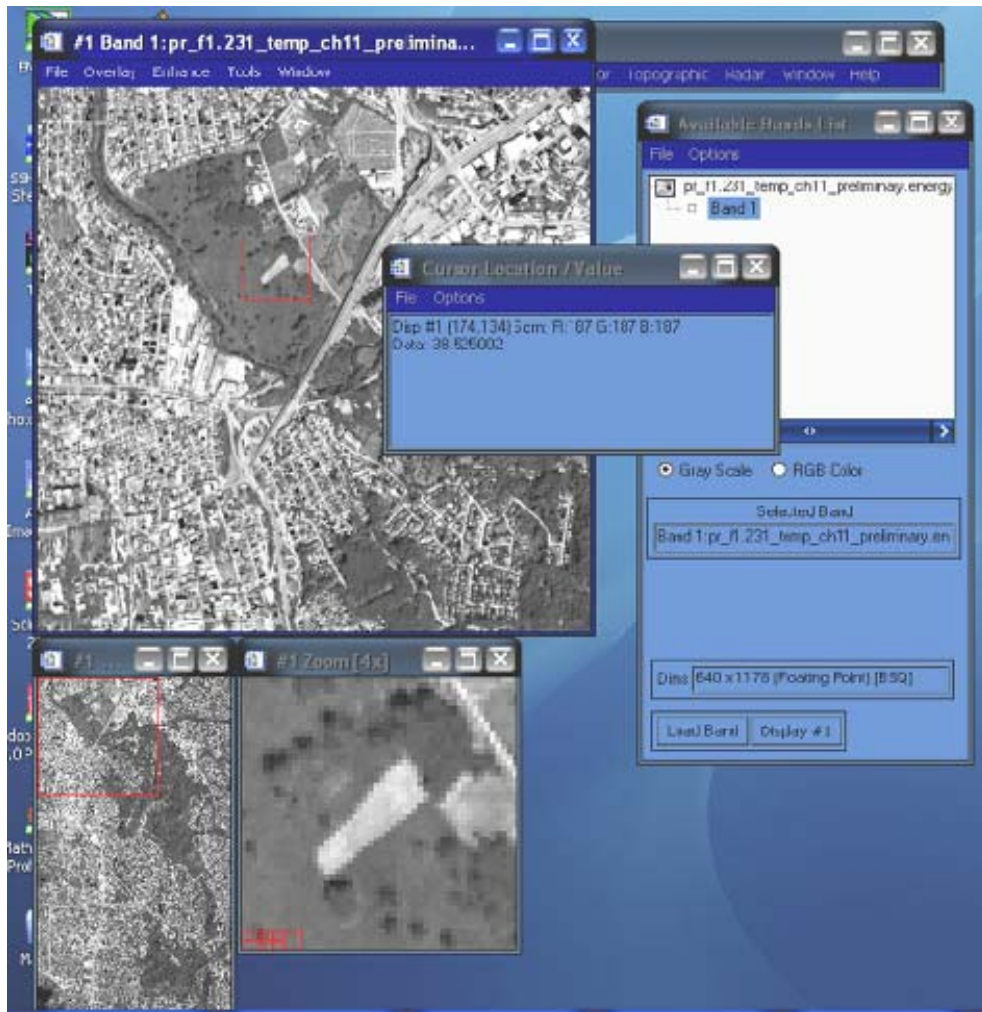


Figure 14 Display of the selected bands.

APPENDIX 2: Additional figures

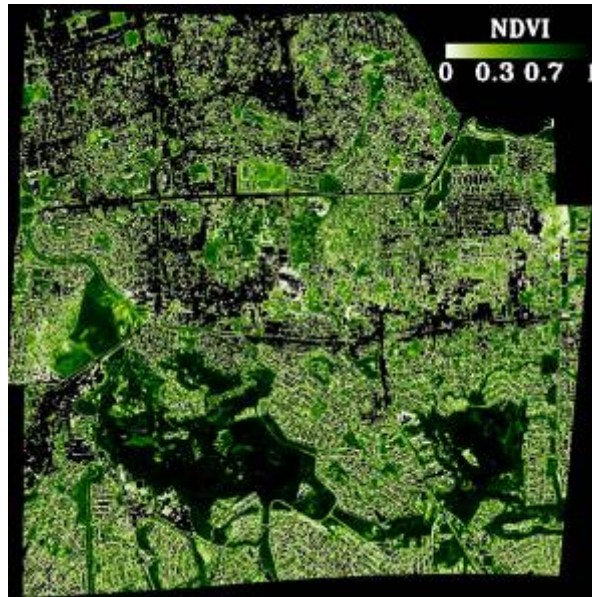


Figure 15 NDVI values for the Hato Rey downtown area.

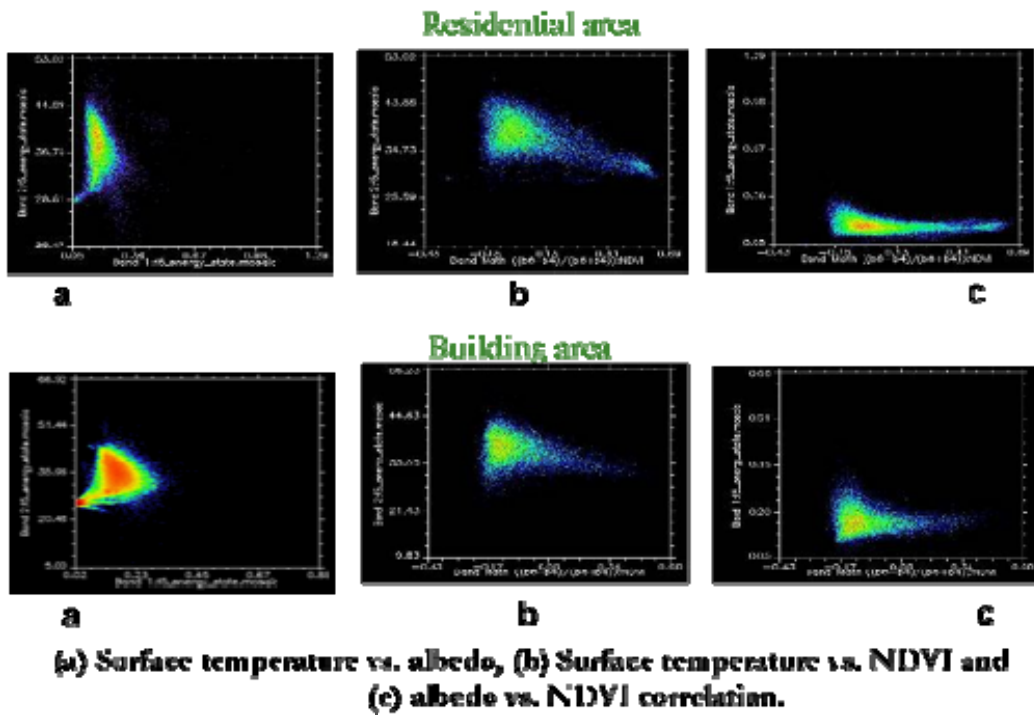
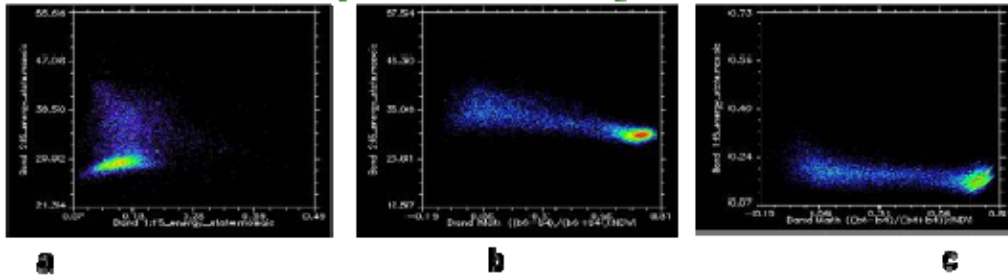
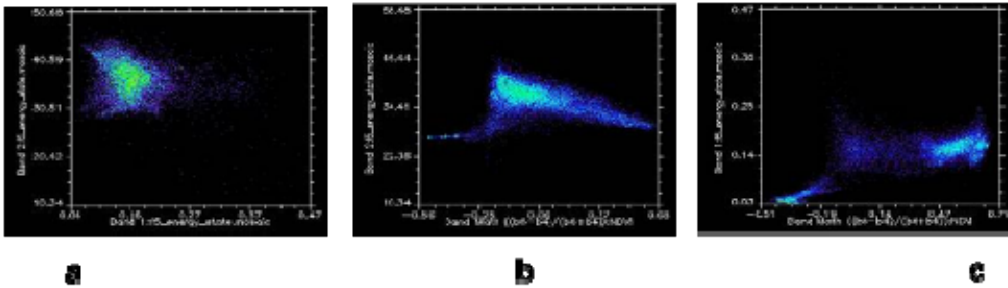


Figure 16 Additional scatter plots for residential and building areas.

Experimental Station: vegetation



Industrial area



(a) Surface temperature vs. albedo, (b) Surface temperature vs. NDVI and (c) albedo vs. NDVI correlation.

Figure 17 Additional scatter plots for vegetated and industrial areas.